16-20 July 2017, Charleston, South Carolina

Correlation of the SAGE III on ISS Thermal Models in Thermal Desktop

Ruth M. Amundsen[1], Warren T. Davis[2], and Kaitlin A. K. Liles[3]
NASA Langley Research Center, Hampton, VA, 23681

and

Shawn C. McLeod[4]
Analytical Mechanics Associates, Inc., Hampton, VA, 23666

The Stratospheric Aerosol and Gas Experiment III (SAGE III) instrument is the fifth in a series of instruments developed for monitoring aerosols and gaseous constituents in the stratosphere and troposphere. SAGE III was launched on February 19, 2017 and mounted to the International Space Station (ISS) to begin its three-year mission. A detailed thermal model of the SAGE III payload, which consists of multiple subsystems, has been developed in Thermal Desktop (TD). Correlation of the thermal model is important since the payload will be expected to survive a three-year mission on ISS under varying thermal environments. Three major thermal vacuum (TVAC) tests were completed during the development of the SAGE III Instrument Payload (IP); two subsystem-level tests and a payload-level test. Additionally, a characterization TVAC test was performed in order to verify performance of a system of heater plates that was designed to allow the IP to achieve the required temperatures during payload-level testing; model correlation was performed for this test configuration as well as those including the SAGE III flight hardware. This document presents the methods that were used to correlate the SAGE III models to TVAC at the subsystem and IP level, including the approach for modeling the parts of the payload in the thermal chamber, generating pre-test predictions, and making adjustments to the model to align predictions with temperatures observed during testing. Model correlation quality will be presented and discussed, and lessons learned during the correlation process will be shared.

Nomenclature

CCD	*Charge Coupled Device*
CMP	*Contamination Monitoring Package*
DMP	*Disturbance Monitoring Package*
ELC	*ExPRESS Logistics Carrier*
ELC-4	*ExPRESS Logistics Carrier 4*
EF	*Electronics fixture*
EOTP	*Enhanced Orbital Replacement Unit Temporary Platform*
ExPA	*ExPRESS Payload Adapter*
ExPRESS	*Expedite the Processing of Experiments to Space Station*
FD	*Finite Difference*
GSFC	*Goddard Space Flight Center*
HEU	*Hexapod Electronics Unit*
HMA	*Hexapod Mechanical Assembly*
HPS	*Hexapod Pointing System*

[1] Aerospace Engineer, Structural and Thermal Systems Branch, Mail Stop 431.
[2] Aerospace Engineer, Structural and Thermal Systems Branch, Mail Stop 431.
[3] Aerospace Engineer, Structural and Thermal Systems Branch, Mail Stop 431.
[4] Aerospace Engineer, Structural and Thermal Systems Branch, Mail Stop 431.

IA	*Instrument Assembly*
IP	*Instrument Payload*
IR	Infrared
IAM	*Interface Adapter Module*
ICE	*Instrument Control Electronics*
ISS	*International Space Station*
LaRC	*Langley Research Center*
LS	*Limb scattering*
MLI	*Multi-layer Insulation*
NASA	*National Aeronautics and Space Administration*
NVP	*Nadir Viewing Platform*
PB	*Power Board*
PSA	*Pressure Sensitive Adhesive*
PWA	*Printed Wiring Assembly*
RMS	*Root-mean-square*
RVDT	*Rotary Variable Differential Transformer*
SA	*Sensor Assembly*
SAGE	*Stratospheric Aerosol and Gas Experiment*
SHC	*Scan Head Cover*
SM	*Scan Mirror*
TC	*Thermocouple*
TD	*Thermal Desktop*
TEC	*Thermos-electric Cooler*
TP	*Test Point*
TTL	*Time to Limit*
TVAC	*Thermal Vacuum*

I. Introduction

The Stratospheric Aerosol and Gas Experiment (SAGE) III instrument is the fifth in a series of instruments developed for monitoring aerosols and gaseous constituents in the stratosphere and troposphere. SAGE III was launched in the SpaceX Dragon vehicle in February of 2017 and mounted to an external stowage platform on the International Space Station (ISS) to begin its three-year mission. SAGE III measures solar occultation, as shown in Figure 1a and lunar occultation in a similar fashion. SAGE III also measures the scattering of solar radiation in the Earth's atmosphere (called limb scattering [LS]) as shown in Figure 1b. These scientific measurements provide the basis for the analysis of five of the nine critical constituents identified in the U.S. National Plan for Stratospheric Monitoring. These five atmospheric components include the profiles of aerosols, ozone (O_3), nitrogen dioxide (NO_2), water vapor (H_2O), and air density using oxygen (O_2).

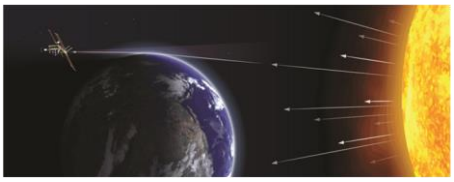

(a) Solar Occultation

(b) Limb Scattering

Figure 1. SAGE III Measurement Techniques.

SAGE III consists of two payloads – the Instrument Payload (IP) and the Nadir Viewing Platform (NVP). The IP, shown in Figure 2, is broken down into several subsystems including the Instrument Assembly (IA), Hexapod Pointing System (HPS), Interface Adapter Module (IAM), Contamination Monitoring Package (CMP), and Disturbance Monitoring Package (DMP). The IA and HPS are existing hardware from the heritage SAGE III on ISS mission while the IAM, CMP, and DMP are being developed. The Nadir Viewing Platform (NVP) is shown in Figure 3. The purpose of the NVP is to orient the IP so that it is nadir-facing; this is required for the IA to collect science data. SAGE III will be mounted on the Expedite the Processing of Experiments to Space Station (ExPRESS) Logistics Carrier (ELC)-4 on the port-facing side of the ELC-4 at site 3, as shown in Figure 4.

Many types of thermal analyses were required for this payload. These included over 120 orbit configurations of the payload thermal model in the Dragon capsule, runs to validate the payload during transfer and in the ISS mounted configuration, runs to determine the worst case orbital parameters for this payload and this location on ISS, standard runs to evaluate the payload thermal behavior during test and in all operational phases, and mapping of thermal results to a structural model to evaluate thermally-induced stress and deflection. In order to expedite this large amount of thermal analysis, many methods were developed to make this thermal model efficient and effective[1,2]. A detailed thermal model of the SAGE III payloads mounted to the ISS was developed at NASA Langley Research Center (LaRC). This model was used for the majority of the analyses. A low-fidelity model was created and delivered to SpaceX and Boeing for integration into their Dragon and ISS models, respectively. SpaceX performed mission-specific analysis for the time between launch and berthing to ISS and Boeing performed detailed analyses to make temperature predictions for the transfer of the IP from the Dragon trunk to the ELC-4.

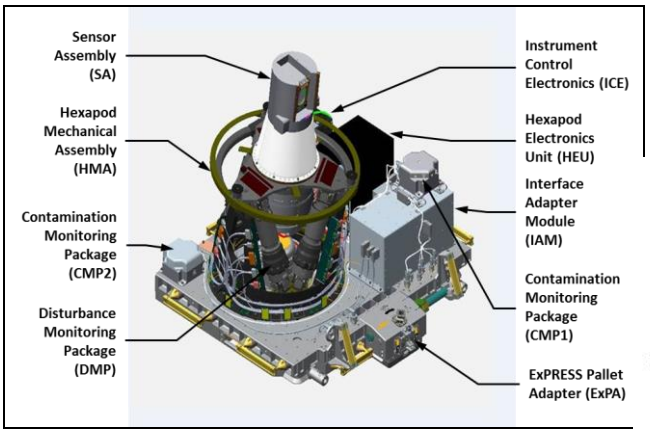

Figure 2. Instrument Payload (IP).

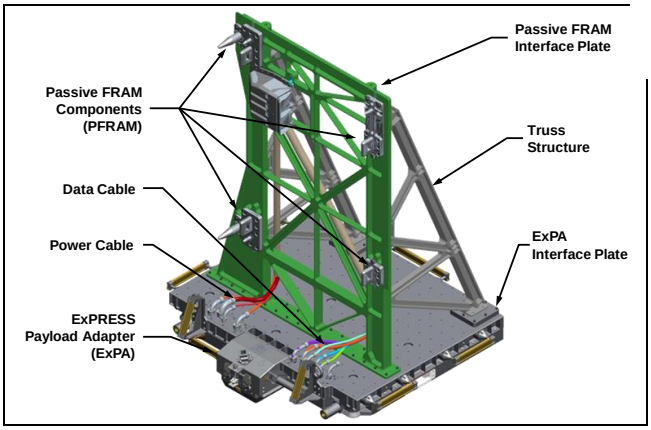

Figure 3: Nadir Viewing Platform (NVP).

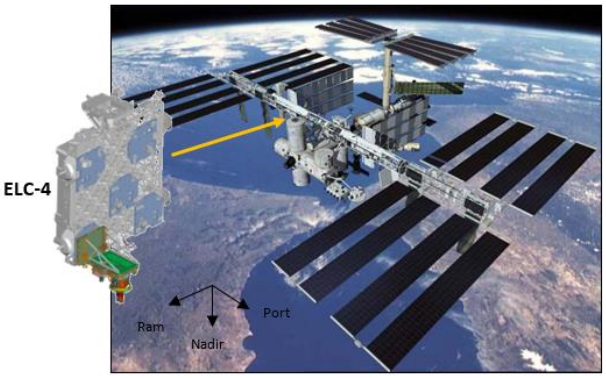

Figure 4: SAGE III Location on ISS.

The IP and NVP designs include various types of thermal hardware including thin-film heaters for survival and operation, multi-layer insulation (MLI) blankets, and thermal tapes. Thermal hardware was selected in order to ensure that the payload would remain within an acceptable temperature range for all phases of the mission.

Correlation of the thermal model was desirable in order to have a model that predicted flight behavior as accurately as possible, however there were no specific NASA or MIL standards that applied to this correlation process.

II. Instrument Assembly Thermal Vacuum Testing and Model Correlation

The SAGE III Instrument Assembly (IA) was the first subsystem tested, because the two components in the IA were heritage hardware that had been developed and built some 20 years earlier for an unflown mission. Thermal vacuum (TVAC) testing was done to ensure that the IA functionality had not degraded in the meantime. The objective of the IA TVAC test was to evaluate the IA subsystem for functionality when exposed to the vacuum and thermal conditions of the space environment. In addition, one hot and one cold cycle dwell were extended to allow thermal balance data to be taken to facilitate correlation of the SAGE III thermal models. Figure 5 shows the IA as it was configured in the 8' x 15' TVAC chamber at NASA Langley Research Center (LaRC) for this test. The Sensor Assembly (SA) was mounted in its support structure, known as the electronics fixture (EF), which mimics the flight conductive interface with the Hexapod Mechanical Assembly (HMA). The Instrument Control Electronics

(ICE) box was mounted as shown in Figure 6; in its bracket which interfaced with an adapter plate via 12 titanium thermal isolators, such that its mechanical and thermal interfaces mimicked the flight-like interfaces. Before the test began, model predictions were produced for all the test conditions; these could be used as a starting point for correlation, and also gave an indication of how long transients would be to achieve quasi-steady-state.

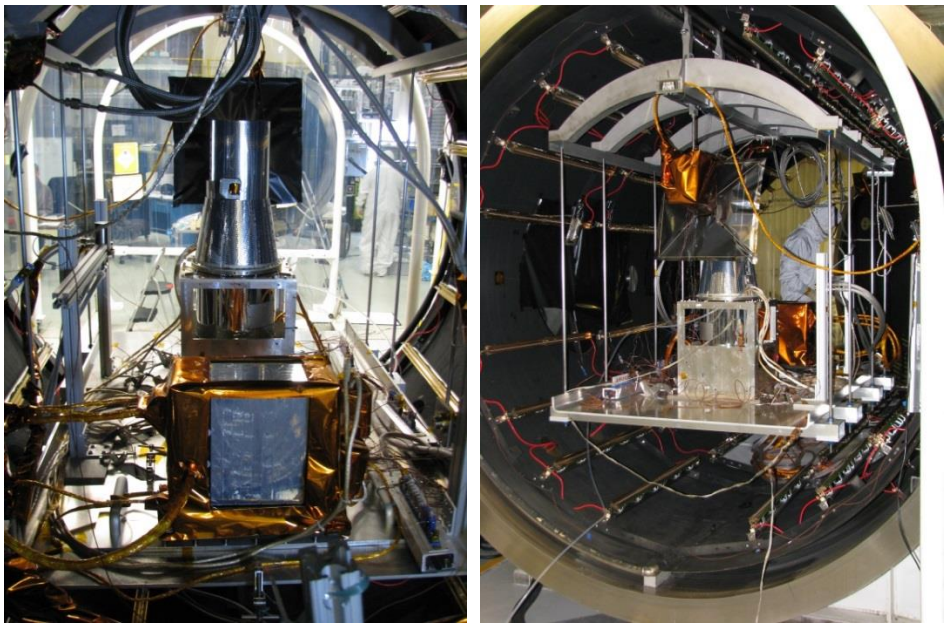

Figure 5. Photos of IA in 8' x 15' TVAC Chamber.

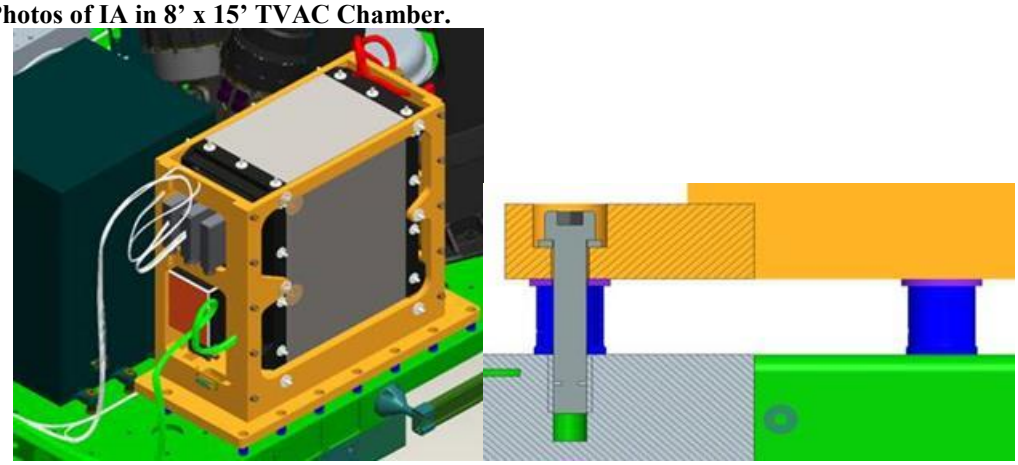

Figure 6: ICE Mounting Configuration.

The data from the TVAC test that was used for model correlation consisted of temperature readings from test facility thermocouples (TC), as well as flight telemetry readings of both temperatures and power from sensors within the IA. The correlation of the sensor assembly model was delayed, because when the initial runs to correlate the model were done, many components were far hotter in test than in the model, even in the unpowered conditions. This led to the discovery that the quartz lamps in the 8'x15' chamber produced a significant fraction of their output in the solar spectrum. Since the thermal model had originally assumed only infrared (IR) radiation, and not enough information on the solar fraction of the lamps was available to incorporate them into the model, correlation using the existing model was not feasible. In order to fully characterize the thermal environment that existed in the chamber during the IA TVAC testing, a chamber characterization test was performed. This test consisted of running the chamber in the same conditions used for the IA test, with test coupons installed to help determine the fraction of the lamp power that was in the solar band, as well as measuring the power used for the lamps. The test determined that roughly 30% of the lamp power was in the solar waveband, and also that there were substantial gradients in the temperatures of the chamber walls. Since the lamps include both solar and IR wavebands, there are two ways to perform the analysis: to run separate radiation cases in both the solar and IR wavebands, or to run the radiation as a

full non-grey analysis using wavelength-dependent properties. In this case, there was not easily available information to allow running this as a non-grey analysis using a full waveband method, although that would probably the more accurate method, so the radiation was run as separate IR and solar waveband cases. Due to these issues with the lamps, the full IP TVAC test was performed using heater plates instead.

After that test was completed, the IA correlation proceeded with the final chamber thermal model from the characterization, which included solar fractions from the lamps as well as chamber wall thermal gradients. Five conditions were run as thermal balance conditions and used for the main correlation of the IA thermal model. These are shown in Table 1. The rationale for these balances is as follows. The unpowered balance is always run first; this allows the model to be correlated to conditions that include only the chamber effects and the quiescent mass of the assembly. In the cold case, a balance is included where only the survival heaters are powered. This allows the correlation with just one change in variable; the application of a well-known and steady power. This is not done in the hot case since the heaters would not activate. Finally, the last balance is with the instrument powered on. This sequence facilitates correlation by allowing the unpowered correlation to correct chamber conditions and connections between parts; in general, the unpowered correlation was used to correct optical properties, chamber and facility hardware, and basic connections between quiescent parts of the instrument. Powering the heaters allows basic correlation of thermal mass and connection of parts that have heaters or are affected by them. And then the powered correlation includes correlation of the instrument powers, as well as thermal mass and connections of final items. In the heater-only and operational balances, the correlation is to the transient, not just to the final condition, which allows good correlation of thermal response. In addition, a brief power-down segment was included after each powered balance. This is a test segment in which the chamber conditions are kept constant, but power to the instrument is removed. This allows a good correlation of the thermal masses. However, the only points that can be correlated are ones that have temperature measurements even when the instrument is unpowered.

Table 1. Thermal Balance Test Points

Test Point (TP)	Condition
TP10a	Unpowered hot balance
TP10b	Operational hot balance
TP11a	Unpowered cold balance
TP11b	Heater-only cold balance
TP11c	Operational cold balance

One of the main factors in correlating the model to the balance test data was the adjustment of contacts between parts. Some of this is due to the history of the SA thermal model. The model was originally built in the 1990's as lumped mass nodes with conductors between them. Those conductors by their nature include both the contact resistance between parts, as well as the part geometry that leads to a thermal resistance between their respective centers of mass. The model was upgraded to true 3D geometry as a part of the thermal team's efforts to develop a fully geometric integrated model; the model was developed in Thermal Desktop. In some cases, when the true geometry was added, the contact between parts was retained from the older model. The parts now incorporated some of the thermal resistance within their own geometry, so most of the contacts between parts could utilize a lower resistance. Thus, as correlation has progressed, many of the contacts between parts have been increased, with resulting lower thermal gradients across the assembly.

The correlation of the model to these thermal balance test points is shown in Table 2. The RMS error for these steady-state comparisons is calculated by determining the error between the test data and the model prediction for each available sensor, and summing those errors as a root-mean-square (RMS) value. This avoids the issue of positive and negative errors canceling each other out. The overall RMS error includes all available sensors, including all facility sensors that apply to the SA, such as the tray and SA mounting stand (support box). The RMS error for only the flight sensors is also given, since that will characterize the accuracy that should be observed in flight. The average error is given simply to give an indication if the model on average tends to be in error too warm or too cold. The overall error is calculated by averaging the values for each test point. For this steady-state comparison, the predictions at the end of the powered transient are compared to the test temperatures at the end of the balance. This steady-state correlation is in general fairly good. Over 500 runs of the model have been accomplished to evaluate and adjust the model correlation. The powered run results (TP11b, TP11c and TP10b) are the stable condition reached at the end of a transient of the correct duration, because that is a much more accurate representation of the test than running a true steady-state. In particular, heater and TEC operation incorporate Thermal Desktop functions which are more reliable in a transient than in steady-state. The overall RMS error of 2.4°C is very good, and includes parts such as the support tray and SA mounting box, which are not meaningful for

future tests or flight. The value of the RMS error over only the flight sensors is the most significant value for future predictions, and 1.4°C RMS error is very good.

Table 2. SA Correlation for Balances

	10a	10b	11a	11b	11c	Overall
Overall RMS error (°C)	1.5	1.7	1.3	2.8	3.9	2.4
AVG error (°C)	0.0	-0.6	0.3	1.1	0.6	0.3
Flight sensor RMS error (°C)	0.6	2.2	0.5	1	1.8	1.4

The model is also compared to the test data in the transients between thermal balance test points. Thus, when the IA came to stability at TP10a, the operational power was turned on, and data was recorded as the IA came to thermal stability at TP10b. Five transients with constant chamber environments exist for correlation, as shown in Table 3. These are the main transients useful for correlation of the entire model. Transients that involve changes in the chamber conditions are not feasible to run with this model, because of having to run a different radiation case and different optical property set each time the lamp powers change. Several smaller transients have been used to correlate portions of the model, for example the Elevation Motor Current Angle Sweep (EMCAS) event data to correlate the elevation motor behavior in the model.

Table 3. Thermal Transients for Correlation

Transient	Duration (hrs)
TP10a to 10b	32
Power off after 10b (cooldown)	6
TP11a to 11b	35.5
TP11b to 11c	27.6
Power off after 11c (cooldown)	4

An example of the final correlated model comparison to the cold heater-only transient is shown in Figure 7. Figure 8 shows an example from the operational transient, of a part which is warmed by an operational heater, so it demonstrates the on-off cycle of the heater.

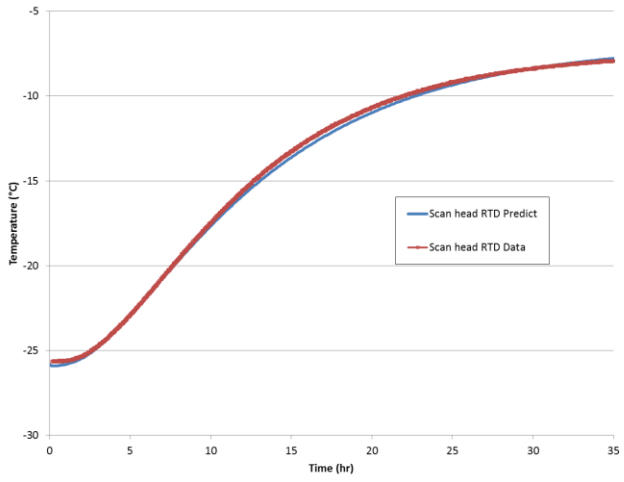

Figure 7. Scan head RTD transient from TP11a to TP11b.

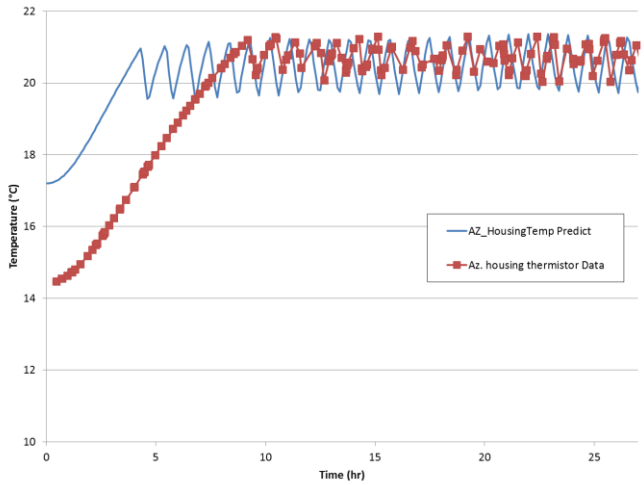

Figure 8. Azimuth housing transient from TP11b to TP11c.

For the transient predictions, a summary of the correlation quality is given Table 4. For transients, the RMS error is calculated by finding the error for each sensor at each time point, and calculating an RMS error for each sensor over the entire timeline. The sensors are then averaged together to produce a single value for the correlation of that transient. For the cooldown transients, the intent is to determine how accurate the change in predicted temperature is, so those errors are calculated as error on the change in temperature, as discussed in the sections on cooldowns. Overall RMS error for the SA flight sensors taken over all the transients is 1.3°C, which is extremely good.

Table 4. Correlation Results for Transients (°C)

	10ab	10b cooldown	11ab	11bc	11c cooldown	Overall
Overall RMS error (°C)	1.4	0.4	2.4	2.8	1.0	2.0
Avg error (°C)	-0.1	0.1	1.3	0.8	-0.7	0.3
Flight sensor RMS error (°C)	1.4	0.6	1.2	1.7	0.9	1.3

III. Interface Adapter Module Thermal Vacuum Testing and Model Correlation

The Interface Adapter Module (IAM) was the second subsystem to undergo TVAC testing. The objectives of the test were similar to the first subsystem test, which were to evaluate the hardware for functionality and performance when exposed to the vacuum and thermal conditions of the space environment, and to collect temperature and power data to support model correlation. Testing was performed in the 6' x 6' TVAC chamber at NASA LaRC. A thermal model representing the IAM SN002 TVAC test configuration was created in Thermal Desktop (TD) version 5.7, patch 9, and is provided in Figure 9. The shroud and front and rear auxiliary platens were temperature controlled via gaseous or liquid nitrogen and served as the primary means for regulating the IAM temperature during the test. For each correlation case, these three elements were modeled as boundary conditions and assigned time-dependent temperature arrays based on measured facility TC data.

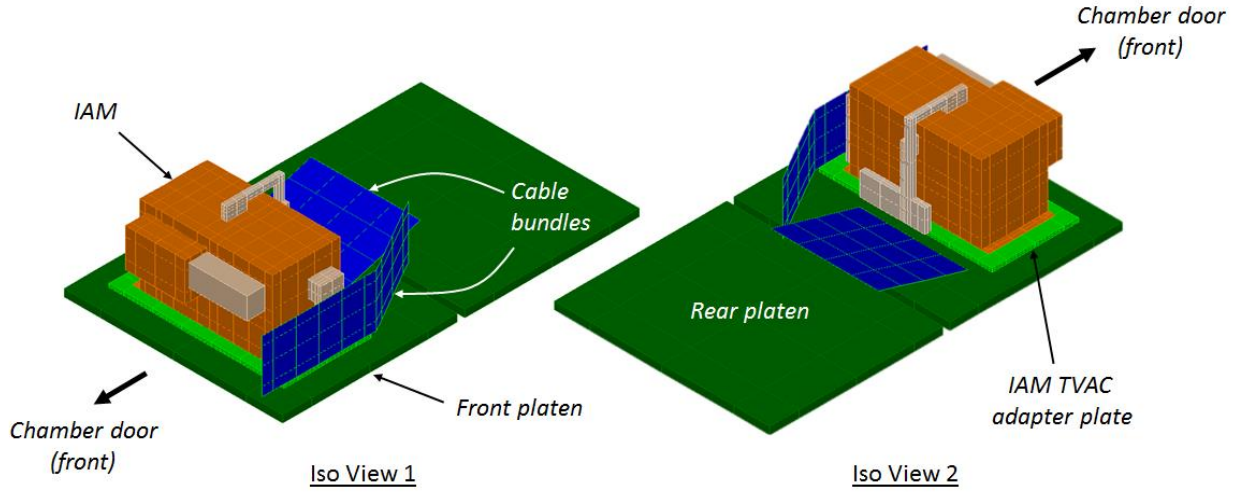

Figure 9. Thermal model of IAM SN002 TVAC test configuration.

Electrical cabling routed from the IAM to the chamber shroud was wrapped with MLI to minimize heat leak from the IAM. Cable bundles that encompassed significant portions of the IAM's view factor were modeled as blocking surfaces and assume MLI thermophysical and optical properties with a Kapton outer layer (e* = 0.03, e = 0.83), per the test configuration. These surfaces were located along the right and back sides of the IAM, as shown in Figure 9, and were coupled to their surroundings via radiation only. The mass of the cables were neglected since the effect on the exterior MLI temperature was insignificant. The IAM was mounted to the IAM TVAC adapter plate (a half-inch thick aluminum plate mounted to the platen) using NuSil CV-2946 conductive silicone per the flight application procedure. The adapter plate was modeled with a FD solid. Two edge nodes were used through the thickness to improve the correlation accuracy of the thermal conductance through the NuSil interface (though any improvement gained over a one-node surface was likely less than 1°C). Since model nodes rarely coincide with temperature sensors, TD temperature measures were placed in the model within close proximity of test TC and flight sensor locations on the IAM and interface plate. The TD program produces an interpolated temperature based on the measure's location relative to nearby nodes. Modeling the test thermal environment was an iterative process. Throughout the modeling effort, hot and cold unpowered cases were run periodically to compare the model to test data and check for accuracy, and adjustments were made accordingly. This process was repeated multiple times to minimize the overall root-mean-square (RMS) error.

The IAM model was correlated to IAM SN002 TVAC test data for hot and cold unpowered and powered test points, including a four-hour cool-down transient. The correlation process started with correlating to unpowered steady-state cases since they have the least number of variables. Powered cases were correlated next, followed by

the transient four-hour cool-down case. Over 200 total analysis runs were executed over the course of the correlation effort.

For correlation to unpowered steady-state cases, data from the hot survival and cold unpowered balance conditions were used. By correlating to the unpowered (and therefore the simplest) cases first, the energy exchange between the IAM and surrounding chamber environment was more accurately captured. This also provided an initial comparison of chassis gradients without the influence of internal power dissipation. This phase of the correlation resulted in initial adjustments to chassis conductors (yielding only ball-park results in some areas) and was critical in generating an accurate model of the test environment. Once the unpowered correlation results produced an acceptable RMS error, model variables controlling interaction between the IAM and the test environment were held constant.

Results of the unpowered steady-state correlation are provided in Table 5. Overall RMS error was less than 2°C for hot and cold cases. Overall average errors indicated that, generally speaking, the IAM model predictions were biased slightly warmer in the hot case and colder in the cold case, which is desirable. Figure 10 shows a sample comparison plot between predicted and measured data for two chassis sensors during the hot unpowered balance condition.

Table 5. IAM Unpowered Steady-State Errors

	Hot Unpowered	Cold Unpowered
Overall RMS Error (°C)	1.7	1.0
Overall Average Error (°C)	0.4	-0.7
Flight Sensor RMS Error (°C)	0.9	0.7

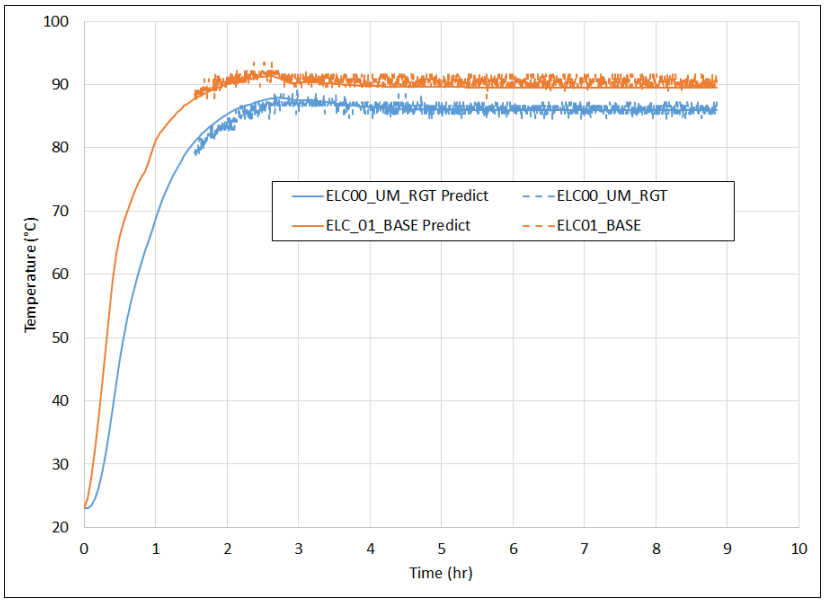

Figure 10. ELC00 and ELC01 IAM chassis predictions vs. test for hot unpowered case.

Powered steady-state cases were correlated to data from hot and cold operational test conditions. Measured current and voltage data from the 28V and 120V power busses were used to find the IAM power dissipation. Power scaling factors were then applied to the model in order to match measured TVAC powers. Since temperature differences are a function of power and conductance, this allowed internal conductors between heat-dissipating components and their surroundings to be tuned such that component predictions matched the test data.

Table 6 shows results of the powered steady-state correlation. Overall RMS error was 1.1°C and 3.1°C for hot and cold cases, respectively. Similar to the unpowered steady-state results, overall average errors indicated that the model was generally predicting warmer in the hot case and colder in the cold case, which again is desirable. Figure 11 shows a sample comparison plot between predicted and measured temperatures of two printed circuit board components during a hot operational test condition. In the middle of the dwell, power was momentarily disabled

during a planned switch from the primary to the redundant system, which explains the dramatic decrease in temperature. Since this was a steady state correlation, efforts were not made to match the transient response. Further, matching this particular response would not provide a worthwhile contribution to the flight model when weighed against the effort required to do so.

Table 6. IAM Powered Steady-State Errors

	Hot Powered	Cold Powered
Overall RMS Error (°C)	1.1	3.1
Overall Average Error (°C)	0.4	-1.5
Flight Sensor RMS Error (°C)	1.1	3.7

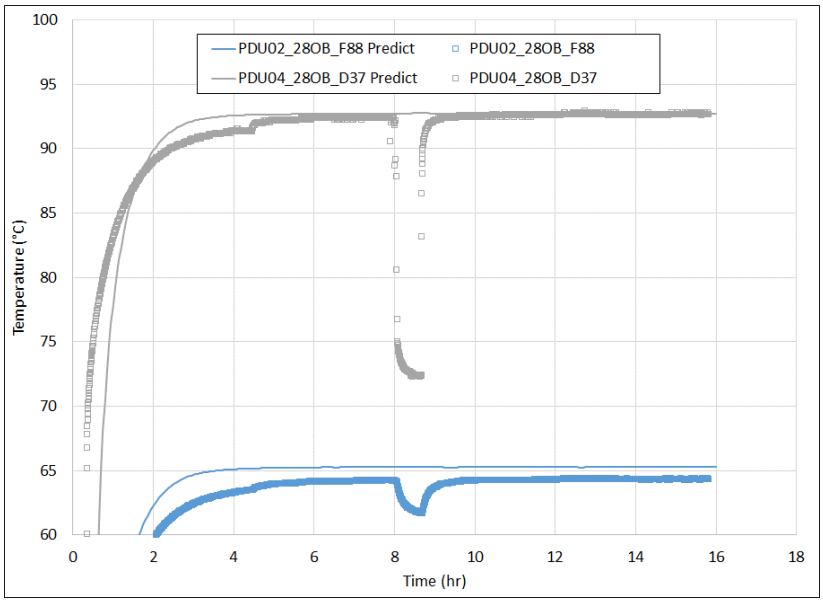

Figure 11. IAM 28V Op board fuse and input diode predictions vs. test for hot powered case.

A four-hour cool-down period following a hot operational test point was used for the transient correlation. During this period, IAM power was disabled and temperatures were allowed to decrease as the chamber control surfaces remained constant. The transient case provided an indication as to whether or not heat capacity adjustments were necessary. Given that the IAM was powered off during this time, temperature data was only available from facility TCs and two flight chassis sensors (ELC00 and ELC01).

Results of the cool-down transient correlation are provided in Table 7. RMS and average errors are presented as calculated over the full transient, as well as by taking the total decrease in temperature over the 4 hour period. The overall RMS error over the full transient was 1.1°C, while the RMS error of the total decrease was 0.6°C. A sample plot showing a comparison between predicted and measured data during the cool-down transient is given is Figure 12.

Table 7. Cool-Down Transient Errors

	Transient	Temp Decrease Over 4 hrs (°C)
Overall RMS Error (°C)	1.1	0.6
Overall Average Error (°C)	0.1	-0.5

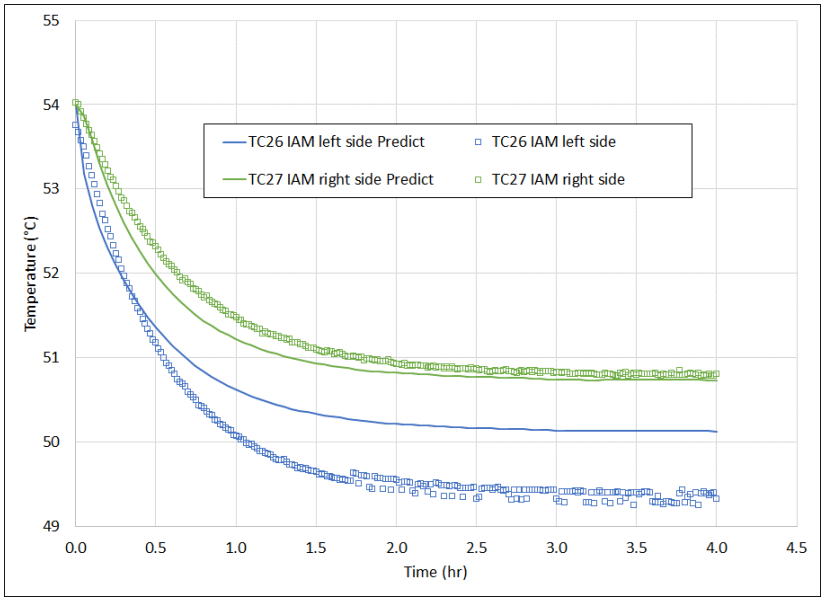

Figure 12. Chassis side panel facility TC predictions vs. test for cool-down transient.

IV. Correlation to Chamber Characterization Thermal Vacuum Testing

For the Instrument Payload (IP) TVAC testing, heater plates were used to achieve temperature plateaus, to avoid the use of the lamps described above. Since these heater plates were a new installation to the facility, a characterization test was run with the heater plates and a dummy payload, to determine if the heater plates could achieve the required plateaus, and allow correlation of the chamber TVAC model, including correct prediction of the gradients on the heat plates. Figure 13 shows the set up in the 8x15' TVAC chamber for this test. After characterization, these same heater plates were used in the IP TVAC test. During this characterization test the payload consisted only of four shells representing some of the SAGE IP components, and a mock ExPRESS Pallet Adapter (ExPA).

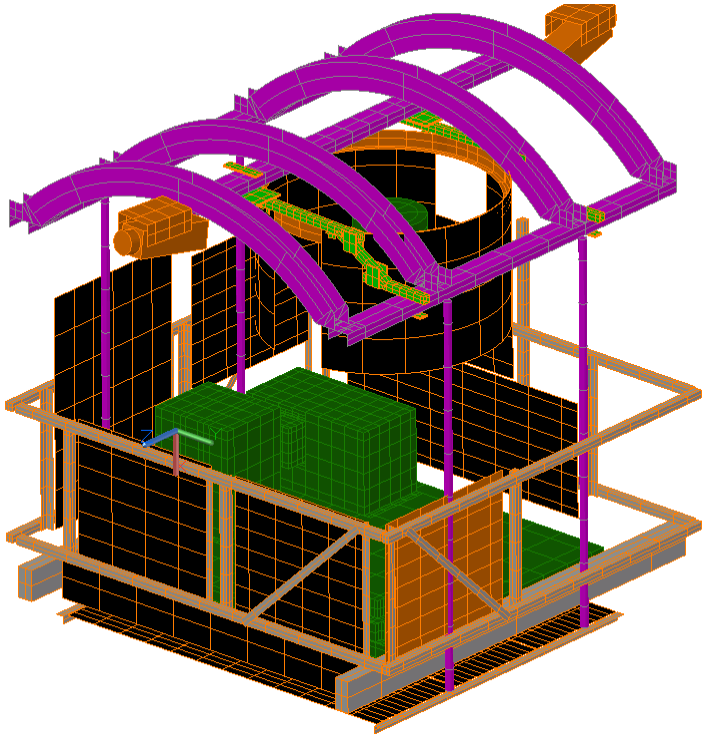

Figure 13. SAGE III Thermal Desktop model, TVAC GSE characterization radiation group.

There were three test points (TP1, 2, 3) and then the chamber was opened and the configuration of the MLI was changed; MLI was removed from both CMP2 heater plates as well as the IAM heater plate, because those plates were not achieving cold enough temperatures in the cold case. After this configuration change, test points 4a and 4b were run.

Since the configuration was different between TP1-3 and TP4, two versions of the thermal model were maintained, one for TP1-3 with all MLI present, and one for TP4 with MLI removed on CMP2 and IAM plates. The TP4 version of the model was then used for the IP TVAC correlation, with the additional change that the control TC for SA heater plate #12 was changed to TC61.

The model was run for all test points, with the appropriate MLI configuration for each one. Over 100 model runs were done with different parameter values to accomplish correlation. Changes to correct the model were as follows.

- Normally, MLI is applied by simply clicking the Insulation tab for the surface. On several of these surfaces, that was found to be ineffective. The reason is that, for example on the three ExPA plates, the MLI beneath them was one continuous piece, and thus exchange with all three heater plates occurred to the inside surface of the MLI. When the MLI is applied in the model on a per-surface basis, there can be no radiative exchange among the backs of the separate plates, and between the inner MLI surfaces facing them. To account for this, in the two relevant locations the MLI was changed from being applied per-surface, to a large independent surface that covered the extent of the affected plates. This was done for the three ExPA plates, and for the combination plate of IAM and CMP1-Z1, as shown in Figure 14.
- Added a radiation conductor between the ExPA plate edges that face each other.
- Contact between heater frames and plates was changed.
- Material for the heater plates was changed to Al 3003 H-14.
- Material for the heaters was changed to Kapton.
- Contact of yoke to chamber was changed.
- Emissivities for heater plates were changed.
- Average emissivity for chamber shrouds was changed.
- Emissivity for GSE shells was changed.
- Control TCs given mass to avoid “banging” behavior.
- Remeshed all heater plates for a finer mesh.
- Changed k factor on TVAC yoke box beams to be the same as mass factor.

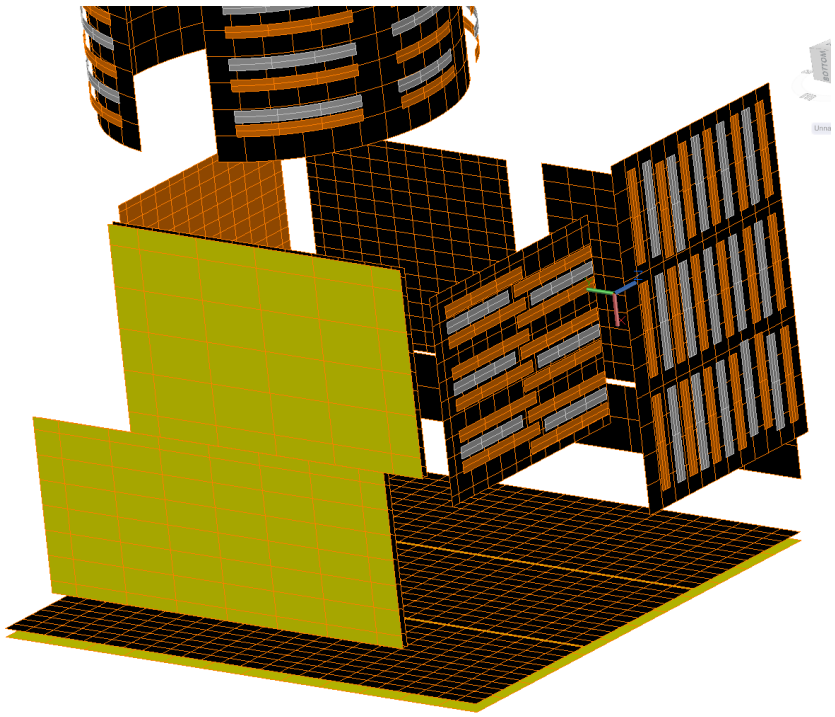

Figure 14. Separate MLI surfaces modeled for TP 1-3.

To accomplish the correlation, at every test point plots such as Figure 15 were made for each heater plate. This shows the difference between prediction and test data for the control TC, as well as the plate gradient, and errors for other TCs on the heater plate (which then shows the errors in gradient prediction). For each test point, a table such as Table 8 was generated to compare predictions of plate temperature and plate gradient with the test data. Table 8 shows an RMS error of the plate predictions of 3.2°C, and 4.1°C on the gradient predictions. One of the major unknowns in correlation was the thermal contact resistance between the frames holding the heater plates, and the contact from the heater plate to the frames. Unfortunately, the thermal sensors were not placed so as to be able to verify the assumptions that were made for these values. A lesson learned from this test was to always place sensors to allow verification of basic assumptions, especially when they affect a large portion of the test hardware. One advantage to having data plotted as in Table 8 was that as new runs were done, the data from each run could be put in the same format, allowing easy determination of how a change in model parameters affected the local and overall errors.

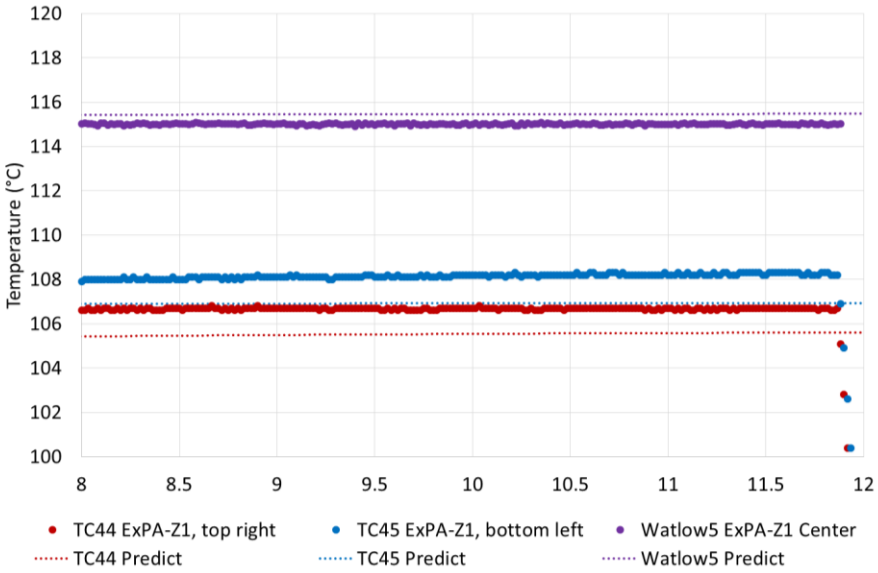

Figure 15. TP1 ExPA Z1 plate thermal predictions compared to test data.

One very valuable action in TP2 was that at different times, three of the heater plates were turned off and allowed to drop in temperature. This is shown in Figure 16; the response of the plates in the model to having the power turned off is gratifyingly close to the behavior observed in test. This shows that the mass and connection of the plates is correct in the model.

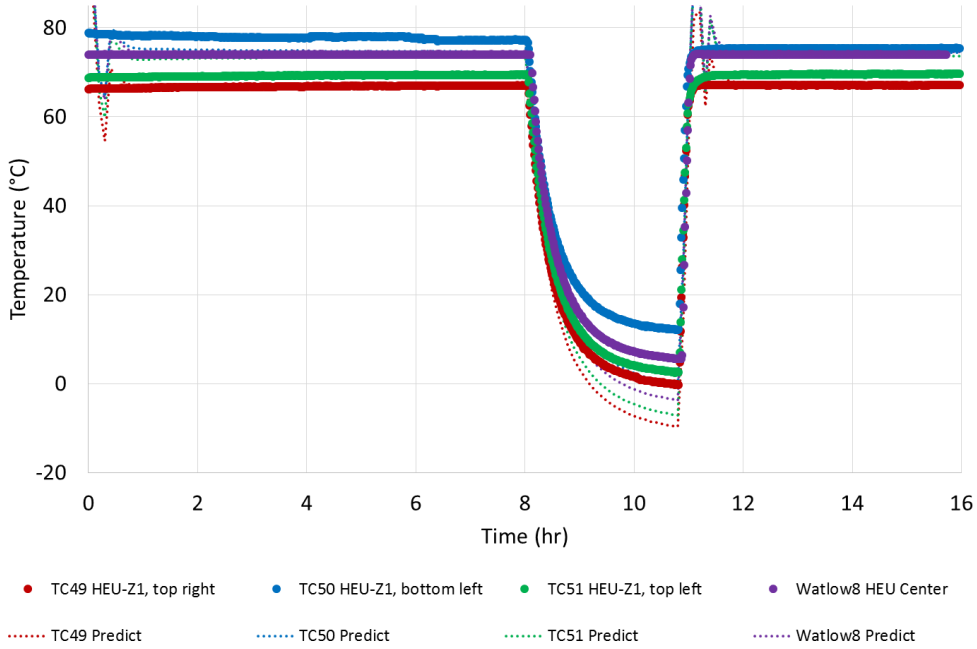

Figure 16. TP2 HEU plate thermal predictions compared to test data.

Table 8. TP4a Hot Op GSE Heater Plate Comparison

Plate	TC Location	TC #	Predicted Temps (°C)		Actual Temps (°C)		Comparison (°C)	
			Temp	Gradient	Temp	Gradient	Temp	Gradient
CMP1-Z1	CMP1-Z1, center	WATLOW1	90.4	9.8	90.0	8.2	0.5	1.7
	CMP1-Z1, top right	35	91.9		88.5		3.4	
	CMP1-Z1, bottom right	36	82.1		85.9		-3.8	
	CMP1-Z1, middle left	37	83.7		81.8		1.9	
CMP1-Z2	CMP1-Z2, center	WATLOW2	90.6	9.7	90.0	9.0	0.7	0.7
	CMP1-Z2, top right	38	89.0		82.1		6.9	
	CMP1-Z2, bottom left	39	81.0		81.0		0.0	
CMP2-Z1	CMP2-Z1, center	WATLOW3	115.0	6.8	115.0	16.2	0.0	-9.4
	CMP2-Z1, top right	40	108.2		101.6		6.6	
	CMP2-Z1, bottom left	41	109.7		98.8		10.9	
CMP2-Z2	CMP2-Z2, center	WATLOW4	115.1	16.7	115.0	15.1	0.1	1.6
	CMP2-Z2, top right	42	98.5		99.9		-1.4	
	CMP2-Z2, bottom left	43	106.8		106.2		0.6	
ExPA-Z1	ExPA-Z1, center	WATLOW5	80.6	7.1	80.0	6.7	0.6	0.4
	ExPA-Z1, top right	44	74.3		75.9		-1.6	
	ExPA-Z1, bottom left	45	73.5		73.3		0.2	
ExPA-Z2	ExPA-Z2, middle right	46	76.5	4.1	75.7	4.3	0.8	-0.2
	ExPA-Z2, middle center	WATLOW6	80.6		80.0		0.6	
ExPA-Z3	ExPA-Z3, center	WATLOW7	80.5	8.1	80.0	8.5	0.5	-0.4
	ExPA-Z3 , top left	47	76.1		75.5		0.6	
	ExPA-Z3, bottom right	48	72.4		71.5		0.9	
HEU	HEU plate, center	WATLOW8	55.7	5.7	55.0	6.6	0.7	-0.9
	HEU plate, top right	49	50.0		49.2		0.8	
	HEU plate, bottom right	50	55.7		55.8		-0.1	
	HEU plate, top left	51	54.9		51.1		3.8	
IAM	IAM plate, top right	52	2.2	16.8	-0.5	6.8	2.7	10.0
	IAM plate, middle right	WATLOW9	-3.8		-4.6		0.8	
	IAM plate, bottom center	53	-10.5		-4.3		-6.2	
	IAM plate, middle left	54	-14.6		-7.3		-7.3	
ICE	ICE plate, center	WATLOW10	30.9	2.9	30.0	2.5	0.9	0.4
	ICE plate, top right	55	32.1		28.7		3.4	
	ICE plate, bottom left	56	29.3		27.5		1.8	
SA-Z1	SA-Z1, center	WATLOW11	40.8	9.8	40.0	9.1	0.8	0.7
	SA-Z1, top right	57	31.0		30.9		0.1	
	SA-Z1, bottom right	58	40.4		39.5		0.9	
	SA-Z1, middle left	59	38.4		37.1		1.3	
SA-Z2	SA-Z2, center	WATLOW12	40.7	6.1	40.0	8.0	0.7	-1.9
	SA-Z2, top right	60	34.6		32.1		2.5	
	SA-Z2, bottom left	61	40.7		40.1		0.6	
						Max	10.9	10.0
						Min	-7.3	-9.4
						RMS	3.2	4.1
						Avg	1.0	

An interesting corollary to this was the behavior of neighboring plates, an example of which is shown in Figure 17. It can be seen that a TC near to the plate that is powered down decreases in temperature, as expected, but a TC further away may actually increase in temperature during this time. The reason for this is that the power used on the plate to maintain the control TC at the correct temperature may increase when an adjacent plate is powered off, which means that temperatures elsewhere on the plate will increase. It gives great confidence in the model that it tracks this behavior correctly. Figure 17 shows the ExPA Z3 plate responding first to the power-down of the IAM heater plate (by TC 48 increasing in temperature), and then to the power-down of the ExPA Z2 plate (by TC 47 decreasing in temperature).

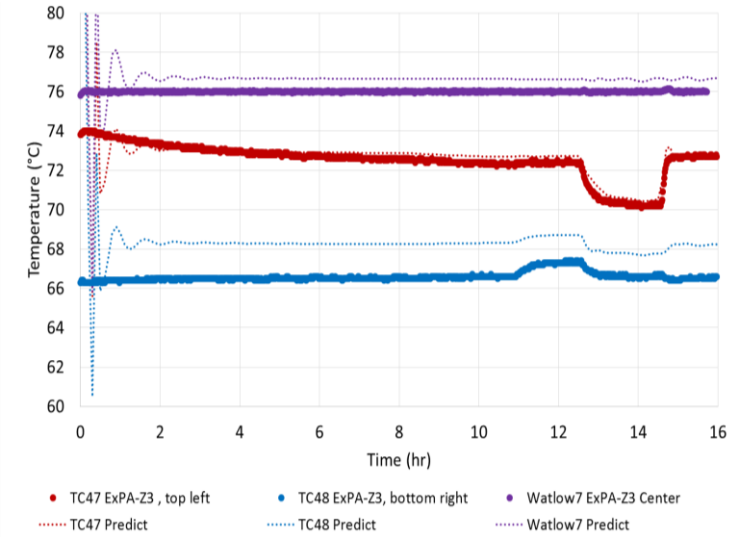

Figure 17. TP2 ExPA Z3 plate thermal predictions compared to test data.

In addition to the prediction of plate data and gradients, the transient behavior of the dummy payload shells was compared between predictions and st, since that would give an indication of the prediction accuracy on the full payload. Figure 18 shows an example comparison of the transient, and the correlation is good.

The overall correlation of the thermal model to these five test points was very good, and gave confidence that the model could be successfully used for the IP TVAC test modeling. For each test point, the RMS error over the test point timeline was calculated, both for all heater plate and frame TCs, and for the GSE shell and mock ExPA TCs (which are more representative of the SAGE III payload behavior in test). Those values are shown in Figure 18; these RMS errors are calculated over the full timeline at each test point rather than at a quasi-steady-state point, and include all sensors rather than just the heater plate sensors. TP4 is most representative of the IP TVAC test, with the same MLI configuration used, so it is helpful that those RMS errors are smaller than TP 1 through 3.

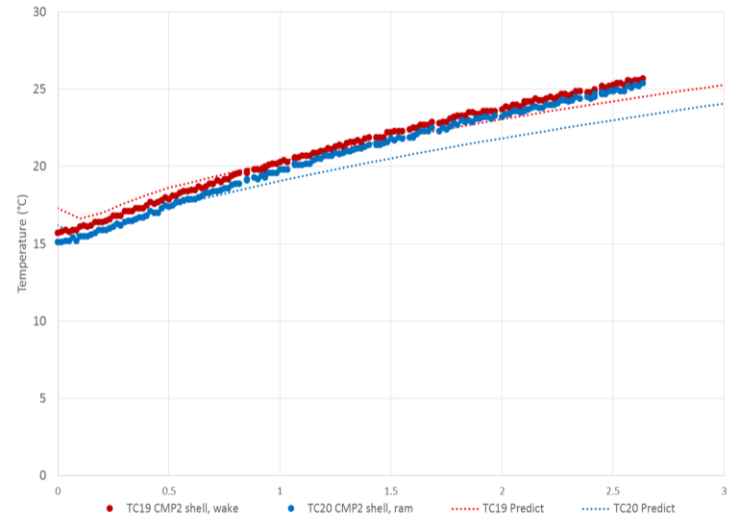

Figure 18. TP4a CMP2 shell thermal predictions compared to test data.

Table 9. RMS Errors over Timelines for Each Test Point

Test Point	Error on GSE shells and ExPA		Error on heater plates and frame (°C)	
	RMS error (°C)	Average error (°C)	RMS error (°C)	Average error (°C)
TP1	4.8	4.5	3.4	2.1
TP2	4.7	0.7	3.4	0.9
TP3	5.8	-1.0	3.9	-1.5
TP4a	1.9	-1.5	2.9	1.4
TP4b	3.8	3.1	3.0	1.4

V. Instrument Payload Thermal Vacuum Testing and Model Correlation

The SAGE III Thermal Desktop thermal model, correlated to the TVAC GSE Characterization test as described above, was used to predict the behavior of the SAGE III IP during thermal vacuum (TVAC) testing. One interesting feature of this model is that the TVAC testing cases were included in the flight productions model, i.e. the model used to predict flight on-orbit behavior. This meant that all model correlation to TVAC testing was automatically included in the flight model. Figure 19 shows the thermal model of the IP within the 8x15 TVAC chamber, with the heater plates used for the test.

The two test points used for the thermal model correlation were the two balances: TP8 for hot balance and TP9 for cold balance. At each test point there was an unpowered balance, a powered balance and an unpowered cooldown; each of those were used for correlation. To fully correlate the behavior of heaters and the thermo-electric cooler (TEC), a step in TP9 was modeled when the heaters were activated and the TEC flipped to the higher set point. In addition, to fully correlate the behavior of the elevation motor during science events, in both TP8 and TP9, orbit simulation events were modeled, where the elevation motor was put through a sequence of position changes to simulate flight science events. In these events, a simulation was performed which included the equivalent of two full orbits of the angles and times for operation of the elevation motor after the payload had achieved thermal balance.

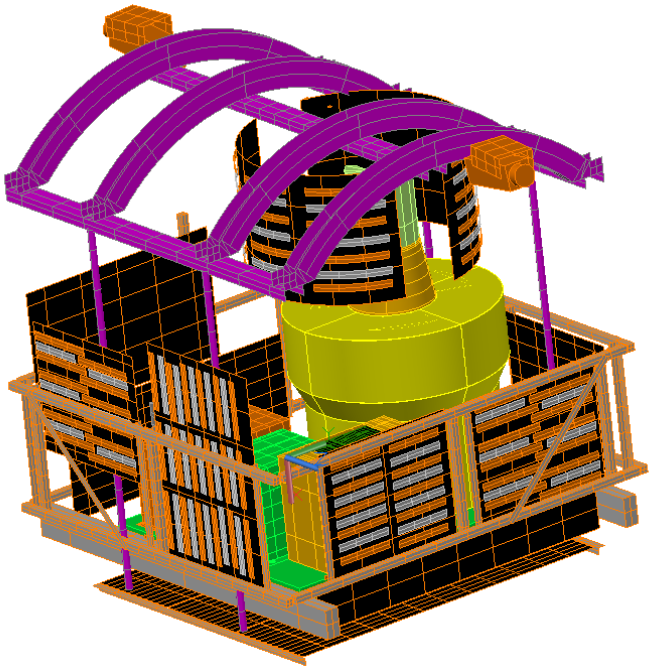

Figure 19. SAGE III Thermal Desktop model, TVAC chamber radiation group.

Measured power for the components was used as far as possible in the correlation. Only transient case runs were used to correlate the model, since the payload is massive enough that in no case did the entire payload come to full equilibrium, so that comparison to a steady-state thermal run would be misleading.

The unpowered cases were evaluated first, because they have the fewest variables and do not include any unknowns regarding the powered components of the payload. However, only the six ELC flight sensors are available from the payload when unpowered. The facility TCs were used for a rough comparison, but because of noise issues with the facility, these were not used in any computation of root-mean-square (RMS) error.

After the model was adjusted to match unpowered cases for TP8 and TP9, the powered balances were used for correlation of the operating payload. During TP9, after balance was achieved in the test, the contingency power bus was activated, which activated the IA and survival heaters. This time period is used for correlation of the behavior of the payload heaters. Finally, in both TP8 and TP9, after balance was achieved, the elevation motor was activated in an orbit simulation mode, and the thermal model prediction was compared to this data. This was done because the elevation motor temperature will most likely be the limiting factor on the duration of limb events in orbit, so having its prediction correlate to data during actual events is critical.

The values changed to achieve correlation included test facility contact of the yoke to the chamber, several emissivity values, conductance of several components to the ExPA, effective emissivity values for several MLI blankets, and several part contact conductance values.

Figure 20 shows an example of a good correlation of a component behavior during the TP8 unpowered balance. It is obviously much more rigorous to show a correlation to the entire timeline as the payload comes to an unpowered balance, rather than just comparing “steady-state” values at the end of balance. Figure 21 shows an example of the timeline comparison for a hot powered case.

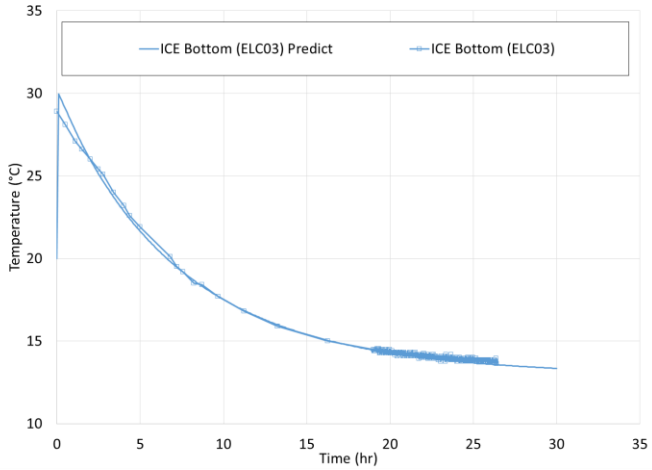

Figure 20. ICE ELC sensor test data compared to prediction for TP8 unpowered balance.

sim was complete, other events were performed with the elevation motor. The current draw for the elevation motor is one of the parameters captured within InControl. The power draw (in W) for the elevation motor is calculated as the resistance (27 ohms) times the current squared (in amps). This measured data was used as the input power for the motor in the model.

With this power timeline input in the model, the response of the elevation motor and RVDT compared very well between the model and test data, as shown in Figure 22. The elevation motor starts slightly too warm, but the size of the temperature increase due to each event is excellent.

One of the most challenging and critical parts of the thermal model correlation was ensuring that the thermos-electric cooler (TEC) behavior was modeled correctly. The TEC needed to control to the correct temperature, have the correct delta between the hot side and cold side (which entails the correct heat dissipation on the hot side), and follow the programmed logic whereby the TEC set point flips up to a higher set point when the CCD shield (representing the hot side of the TEC) goes above a certain temperature point. One issue that arose was that the standard method for modeling a TEC in Thermal Desktop led to thermal case runs with extremely long execution times, when the flip behavior was implemented in the model. To avoid this, the behavior of the TEC in the model was modified such that the power applied to the TEC was proportional to the square of the ratio that defined the difference of the TEC cold side from its set point. Originally the power applied had a direct proportionality to that ratio, and "ringing" behavior would occur which de-stabilized the model solution

The elevation motor is a critical component that warms up appreciably during science events. As such, a section of the TVAC test was devoted to performing an orbit simulation that, for the time period of 2 orbits (3 hours) would have the elevation motor traverse exactly the same angle excursions as it would during a normal orbit. After the payload came to balance in the powered case, the first action was to run an orbit simulation for the elevation motor. The purpose of this was to allow good correlation of the elevation motor behavior during the performance of flight-like science events. The sequence of events in this simulation was sunset, lunar, sunrise, limb (repeated twice). During the hot balance orbit sim, each limb event was 2 minutes long. After the orbit

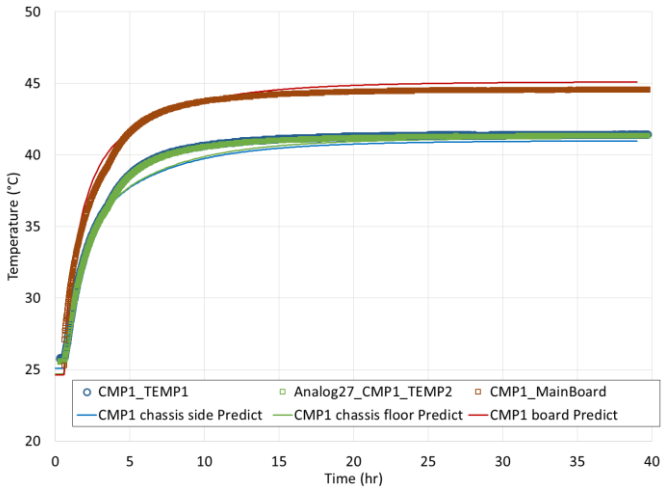

Figure 21. Hot powered balance (TP8) comparison of CMP1 temperatures.

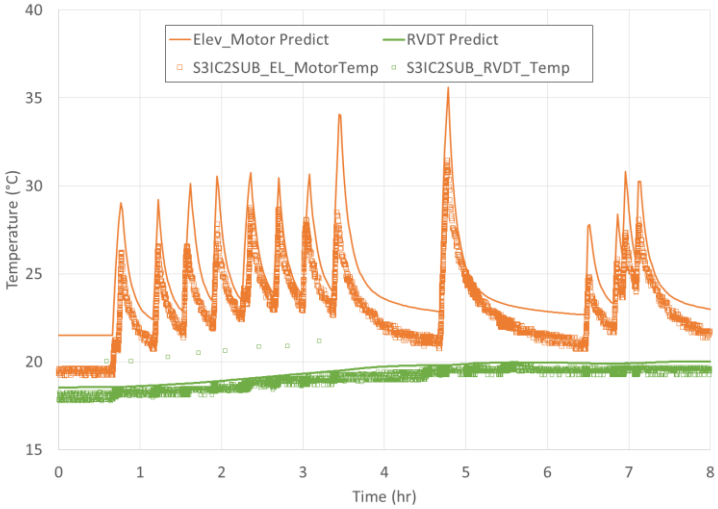

Figure 22. Hot orbit simulation (TP8) comparison of elevation motor and RVDT temperatures.

and brought time step size to a very low value, which made solution times extremely long.

Once the issue of long run time was addressed, the TEC behavior in the model was compared to a test segment where the TEC had flipped up to a higher set point under software automatic control. This occurred in TP9 when the heaters were activated and the TEC flipped to its higher set point. Another benefit of using this segment of the test for comparison was that the behavior of the model when heaters were activated could be compared to the test data. As shown in Figure 23, the comparison of the CCD (cold side of the TEC) when the temperature flips is perfect, indicating that the software programming that changes the TEC set point is correctly modeled. The CCD shield (hot side of the TEC) is predicted slightly too low, but in the hot case (TP8) this CCD shield prediction was perfect – and the hot case correlation took precedence. The comparison of the spectrometer as the heaters activate is excellent as shown in Figure 24.

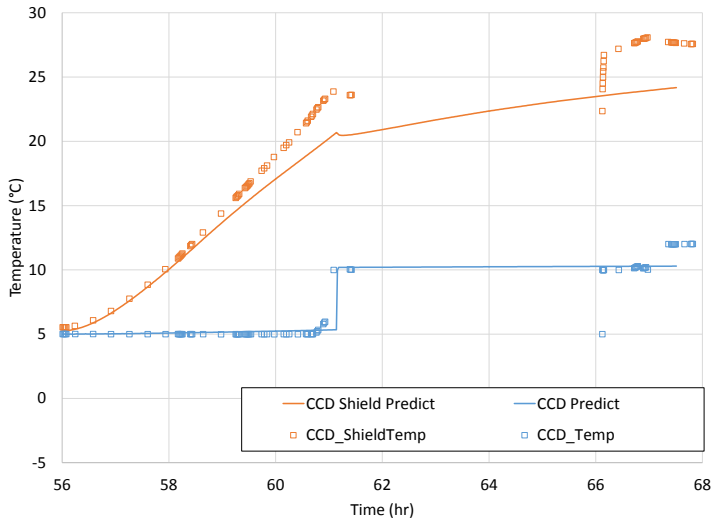

Figure 23. TP9 with heaters activated: comparison of CCD and CCD shield temperatures.

the slope predictions are excellent. This gives good confidence that the model can accurately predict the change in temperature over the unpowered durations on-orbit. On both ISS and Dragon, there is the potential for unpowered durations, and additionally there are planned unpowered durations during the robotic transfer of SAGE III from the Dragon trunk to the ELC-4 final mounting site. It is important to be able to well-predict the behavior of the payload in these unpowered situations, so that the flight predictions can ensure that the payload does not go outside required limits during these times.

The cooldowns were 6-hour periods where all power was turned off to the payload, but the chamber conditions were maintained constant. This allows evaluation of how well the model predicts the fall in temperature of the components in an unpowered condition. This is critical because the payload must survive several unpowered conditions both during transfer to ELC-4, and at times during its lifetime on ISS. The slope of the curves during cooldown looked very good; Figure 25 is shown as an example. Some components did not start at exactly the correct temperature in the model (it being too complex to reproduce all testing and effects that occurred before cooldown), but the behavior in cooldown looks accurate. In particular for components that are starting near the correct temperature,

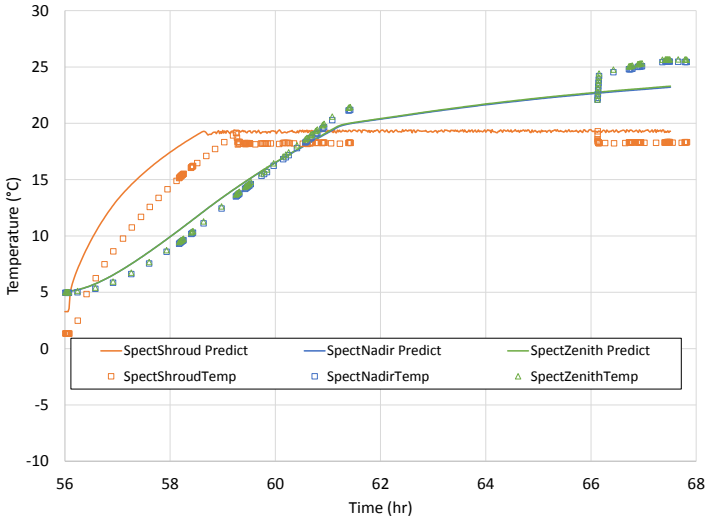

Figure 24. TP9 with heaters activated: comparison of spectrometer temperatures.

Overall, the correlation of the SAGE III thermal model to the IP TVAC testing was excellent. The behavior of the TVAC chamber, heaters, payload response to power, TEC operation, and elevation motor were all well-predicted. Changes to the flight predictions based on correlation were small, and were benign in all cases. The overall errors for each of the balances and cooldown test segments are shown in Table 10; cooldown temperatures are shown as a delta from the start temperatures, since start temperatures in the model were not always correct. It is truly remarkable that this thermal model, which includes not only heritage thermal models from 20+ years ago, as well as models from NASA LaRC, Alenia and NASA JSC integrated into a single model, has correlation to an RMS error of 2.4°C and an average error of less than 1°C. This certainly gives confidence that the flight predictions should be within a 5°C uncertainty band; and in fact, now that SAGE III is on-orbit, the flight temperatures have been observed for most of the model to be within 2°C of predictions. Also the shapes of the curves as conditions changed were very well-represented in the model, which gives confidence that the physical behavior is being modeled correctly. Based on this evidence, the correlation of the SAGE III IP to TVAC testing is complete and is considered highly successful.

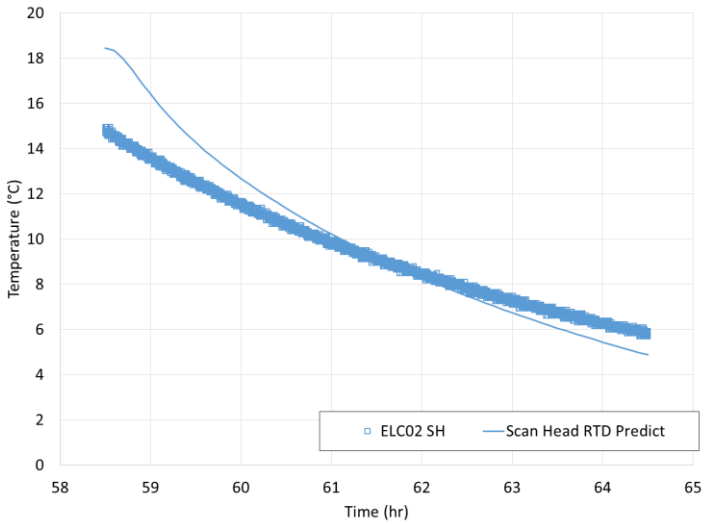

Figure 25. TP8: Hot unpowered cooldown comparison of scan head temperature.

Table 10. Summary of Overall Model Correlation Errors, including IAM Correlation

Test segment	RMS error for flight sensors (°C)	Avg error for flight sensors (°C)
TP8 Hot Unpowered Balance	1.1	-0.9
TP9 Cold Unpowered Balance	2.7	-0.1
TP8 Hot Powered Balance	1.7	0.1
TP9 Cold Powered Balance	2.8	0.8
TP8 Hot Unpowered Cooldown (Delta)	3.2	-2.3
TP9 Cold Unpowered Cooldown (Delta)	2.6	-1.2
Overall average	**2.4**	**-0.6**

VI. Conclusion

This paper has discussed many of the challenges and processes for correlating thermal models to TVAC testing. Some of the central issues described are summarized here. In general, use of quartz lamps in TVAC can make correlation more difficult if the lamps have a substantial output fraction in the solar waveband. IR heater plates are easier to correlate to and to control. If quartz lamps are used, the analysis should probably be done using wave-length dependent radiation properties. In doing correlation, best practice is to proceed from simple to complex. This would mean correlating to unpowered hot and cold cases before correlating to cases with active heaters, and correlating to heater-only cases before correlating to fully-powered cases. It is important to correlate to both hot and cold unpowered cases (when available) before proceeding, because different behaviors may be important in one and not the others, so correlating to only one may lead to inaccuracies.

A simple way to improve correlation is to implement changes in test conditions that are imposed solely for improving model correlation such as turning off a heater plate or turning off power to the payload, with steady environment conditions. This allows precise identification of behaviors that correspond to the items turned off.

The action of powering down the payload briefly, even if the changed condition is not allowed to progress as far as steady-state, can be valuable to compare the predicted transient to the test transient. There are many components of heater behavior that are very useful to measure the modeling quality of the heaters. Items that can be compared between prediction and test are the initial transient behavior on heater power-on, the temperature delta or deadband over which the heater and associated sensors oscillate, and the frequency of oscillation.

TD Measures were found to be valuable to simulate TCs, and allow altering the underlying mesh to improve correlation without disturbing the sensor location; also, sensors can be precisely placed in the desired location, and the underlying temperature will be interpolated at the sensor location. The behavior of an older, slightly degraded TEC was modeled successfully by modifying the TEC power dissipation equation within the TD logic.

Characterizing new TVAC chamber equipment can be very valuable to do separately, before insertion of an uncorrelated payload for testing. If at all possible, always place some sensors so as to verify some of the basic assumptions in the thermal model such as contact conductances. In specific cases, it may be inappropriate to apply MLI using the TD checkbox – in particular, when two surfaces with very different temperatures are covered with the same piece of MLI.

The analysis was greatly facilitated by use of a single model that included all flight cases as well as TVAC cases. This allowed the correlation to TVAC to be automatically captured in the production flight model, and applied quickly and easily to flight predictions. For measuring the model correlation quality, the RMS error was the most valuable as single model quality measure. Averaging the RMS error across multiple sensors and multiple cases allows the analyst to have a single measure of correlation as many correlation trial cases are run. Correlation of a complex model like this to a TVAC test campaign may require several months of work, but this effort has been found to be worthwhile both in correlating the model behavior for flight predictions, as well as identifying systemic errors or issues that may apply to more than one test program.

The model quality for the SAGE III thermal model was very good; in TVAC testing the RMS error was less than 3°C overall. That has been reflected in the first data coming back from flight, and the the initial flight data shows good agreement with predictions.

Acknowledgments

The authors would like to acknowledge the support from the SAGE project personnel, as well as the support from the Systems Integration and Test branch in accomplishing this TVAC testing.